Environmental Science and Ecotechnology 21 (2024) 100390

Contents lists available at ScienceDirect

Environmental Science and Ecotechnology

journal homepage: www.journals.elsevier.com/environmental-science-and-ecotechnology/

Original Research

Enhanced nitrate reduction in hypotrophic waters with integrated photocatalysis and biodegradation

Bingjie Xue [a, 1], Li Tian [a, 1], Yaqi Liu [a], Lingxiu Peng [a], Waheed Iqbal [b], Liangzhong Li [c, **], Yanping Mao [a, *]

[a] College of Chemistry and Environmental Engineering, Shenzhen University, Shenzhen, 518071, PR China
[b] School of Chemistry and Chemical Engineering, Northwestern Polytechnical University, Xi'an, 710072, PR China
[c] Guangzhou Institute of Energy Conversion, Chinese Academy of Sciences, Guangzhou, 510640, PR China

ARTICLE INFO

Article history:
Received 28 May 2023
Received in revised form
5 January 2024
Accepted 7 January 2024

Keywords:
Nitrate reduction
Photocatalysis
Activated sludge
Biodegradation
Metabolic pathway

ABSTRACT

Addressing nitrate contamination in water bodies is a critical environmental challenge, and Intimately Coupling Photocatalysis and Biodegradation (ICPB) presents a promising solution. However, there is still debate about the effectiveness of ICPB in reducing nitrate under hypotrophic conditions. Further research is needed to understand its microbial metabolic mechanism and the functional changes in bacterial structure. Here we explored microbial metabolic mechanisms and changes in bacterial structure in ICPB reactors integrating a meticulously screened TiO_2/g-C_3N_4 photocatalyst with biofilm. We achieved a 26.3% increase in nitrate reduction using 12.2% less organic carbon compared to traditional biodegradation methods. Metagenomic analysis of the microbial communities in ICPB reactors revealed evolving metabolic pathways conducive to nitrate reduction. This research not only elucidates the photocatalytic mechanism behind nitrate reduction in hypotrophic conditions but also provides genomic insights that pave the way for alternative approaches in water remediation technologies.

1. Introduction

Nitrate (NO_3^-) concentration in aquatic systems increased dramatically worldwide due to excessive use of nitrogen fertilizers, inadequate treatment of sewage discharge, and waste effluents from certain industries [1]. Meanwhile, nitrate in water is highly soluble and stable, making reduction extremely challenging [38]. Nitrate accumulation in water resources promotes biological growth and algal blooms, leading to the eutrophication of water bodies [30]. Additionally, the excessive nitrogen concentration in drinking water sources has toxicological effects on humans. High nitrate concentrations and its intermediate product, nitrite (NO_2^-), which is reduced by nitrate in the human gut, can cause methemoglobinemia and other cancers [30]. Therefore, finding economical and efficient treatment processes to remediate nitrate-contaminated water bodies is imperative to protect public health and realize sustainable environmental development.

Photocatalysis is a promising solar-driven advanced oxidation process (AOP) that can be activated by solar irradiation, producing highly reactive photo-generated charge pairs that react with pollutants. Increasing photocatalytic oxidation efficiency through reduced electron and hole complexity is one of the key steps in improving its performance [21]. Regarding nitrate reduction, photocatalysis is a promising technology since it can reduce nitrate to harmless nitrogen. Introducing hole scavengers and a low pH can reduce nitrate more efficiently [8,19,21]. However, the maintenance of an acidic condition and the addition of hole scavengers increase the operational costs. In contrast to photocatalysis, biological denitrification is environmentally benign and feasible to implement, which can be divided into three stages: ammonification, nitrification, and denitrification. Although the biological method has been successfully applied to practical wastewater treatment, several shortcomings still need to be addressed. The biological denitrification process usually occurs in the second half of the wastewater treatment and, therefore, suffers from a shortage of organic carbon sources. To maintain the biological process, it is necessary to introduce an additional carbon source to serve as the

* Corresponding author.
** Corresponding author.
E-mail addresses: lilz@ms.giec.ac.cn (L. Li), maoy@szu.edu.cn (Y. Mao).
[1] These authors have contributed equally to this work and share first authorship.

https://doi.org/10.1016/j.ese.2024.100390

electron donor. This action, however, may result in an overgrowth of microorganisms, subsequently leading to secondary pollution [5].

In recent years, intimately coupling of photocatalysis and biodegradation (ICPB) has shown great potential in degrading various aquatic pollutants. In the ICPB system, the photocatalyst is loaded on the surface of the porous carrier, and the biofilm is cultivated inside the carrier. Photoelectron transfer occurs between the microorganism and photocatalyst due to light irradiation [28]. When a photocatalyst absorbs photon energy exceeding the band gap of the valence band (VB), it facilitates the excitation of electrons, enabling their transition from the VB to the conduction band (CB). This transition results in the generation of photogenerated electrons and holes. Subsequently, these photogenerated electrons and holes can react with substances on the surface of the photocatalyst, producing a series of highly reactive radicals such as OH· and O_2· [42]. These radicals can react with recalcitrant pollutants, converting them into intermediates more easily assimilated by microorganisms [20]. The products of photocatalysis are transferred to the interior of the carrier and degraded by the attached microorganisms for further mineralization into the water and carbon dioxide (Fig. 1). In addition, microorganisms can use electrons generated by the light-induced photocatalyst to maintain their own metabolism, stimulate growth and regulate the community structure [6,12,24].

ICPB has been widely studied to degrade recalcitrant pollutants such as antibiotics [6,13,20,25,32,34,43], dyes [7,14–17,35], and polycyclic aromatic hydrocarbons [3,23,37,48]. Recently, a self-photosensitized nonphototrophic *Thiobacillus denitrificans* (*T. denitrificans*-CdS) was proposed, capable of NO_3^- reduction and N_2O production under light drive [4]. An ICPB system using TiO_2/g-C_3N_4 as a photocatalyst was built, proving that it could efficiently reduce nitrate under visible light irradiation [41].

In the early stages of research, photocatalysts used in ICPB were typically excited by ultraviolet (UV) light [15,36]. However, Zhou et al. discovered that ICPB, when exposed to visible light, exhibited superior performance in treating phenolic wastewater compared to its UV-irradiated counterpart [47]. This advantage arises from the fact that microbial cells tend to absorb UV light, leading to cell membrane damage and cell death. In contrast, visible light protects the microbial community within the porous carrier while enhancing the secretion of extracellular polymeric substances. Consequently, using visible light-induced photocatalysis in the ICPB system can achieve higher degradation efficiency for recalcitrant pollutants, coupled with improved pollutant mineralization capabilities. Furthermore, it safeguards the integrity of the biofilm, enhances solar energy utilization efficiency, and reduces treatment costs.

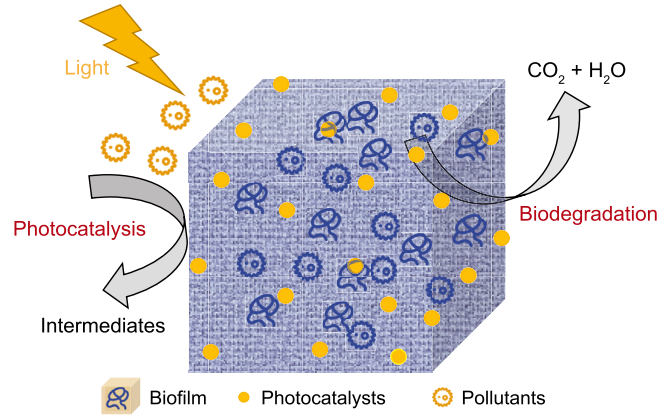

Fig. 1. The mechanism diagram of intimately coupling photocatalysis and biodegradation (ICPB).

g-C_3N_4, a novel visible-light non-metallic photocatalytic material, demonstrates excellent visible-light catalytic performance at non-nanometer scales, characterized by its stable chemical properties, straightforward synthesis, and non-toxic nature. Furthermore, harnessing the synergistic effects between g-C_3N_4 and semiconductors, such as ZnO and TiO_2, promotes the efficient separation of photogenerated electrons and holes, enhancing their photocatalytic performance [46]. Consequently, in this study, g-C_3N_4 and TiO_2 were selected as composite photocatalysts and applied in the ICPB system.

ICPB may provide a new solution to deal with the nitrate issue. In wastewater treatment plants, the nitrogen removal efficiency usually cannot be guaranteed, especially when the organic carbon is deficient since most denitrifiers are heterotrophic microorganisms. The lack of an organic carbon source greatly inhibits nitrate reduction. However, the effectiveness of ICPB in reducing nitrate under hypotrophic conditions is still unclear, and the metabolic mechanism and functional changes of the microbial community in ICPB need further investigation as well.

This study intends to screen out high-quality photocatalysts and functional bacteria and further reveal their synergistic efficiency and metabolic mechanism of nitrate reduction in ICPB. The results may provide a scientific basis for the practical application of ICPB in nutrient removal.

2. Materials and methods

2.1. Preparation of photocatalysts

The analytical grade reagents used in this study were purchased from Shanghai Aladdin Bio-Chem Technology Co. Ltd (Shanghai, China). Potassium nitrate was used as a nitrate source. The solutions used throughout the experiment were prepared using ultrapure water. The preparation of g-C_3N_4 was conducted through direct thermal condensation of precursors (thiourea, melamine, dicyandiamide, and urea) at 550 °C in the muffle furnace for 4 h. The subsequent yellow products were labeled as TCN, MCN, DCN, and UCN, depending on the type of precursor, and grounded into powder with the help of an agate mortar and pestle before further use.

The TiO_2/g-C_3N_4 nanocomposite photocatalyst was prepared under high-temperature calcination by adjusting the weight ratios of P25 TiO_2 and g-C_3N_4 as 1:2, 1:1, and 2:1 and mixed in 50 mL ultrapure water. The mixture was continuously stirred with a magnetic stirrer for 16 h and then centrifuged at 4000 r min^{-1} for 10 min. After centrifugation, it was dried in an oven at 60 °C and then calcined in a muffle furnace at 450 °C for 1 h. Finally, the product was ground into powder. Twelve TiO_2/g-C_3N_4 nanocomposite photocatalysts were prepared by adjusting the weight ratios of two photocatalysts.

2.2. Coating of photocatalysts

This study used polyurethane sponge cubes (Jiangsu Aqin Environmental Protection Technology Co., Ltd., China) with dimensions of 7.5×7.5×7.5 mm and 95% porosity containing 2–7 mm macropores. The loading process was as follows: 2.0 g TiO_2/g-C_3N_4 nanocomposite powder was dispersed in 100 mL of anhydrous ethanol, followed by 2 mL of concentrated nitric acid added dropwise in the mixture. The mixed solution was ultrasonicated for 30 min. After sonication, 2.0 g of polyurethane sponge cubes were added to the solution. After that, the mixture was placed in an oven at 60 °C and stirred with a glass rod every 30 min until all the liquid

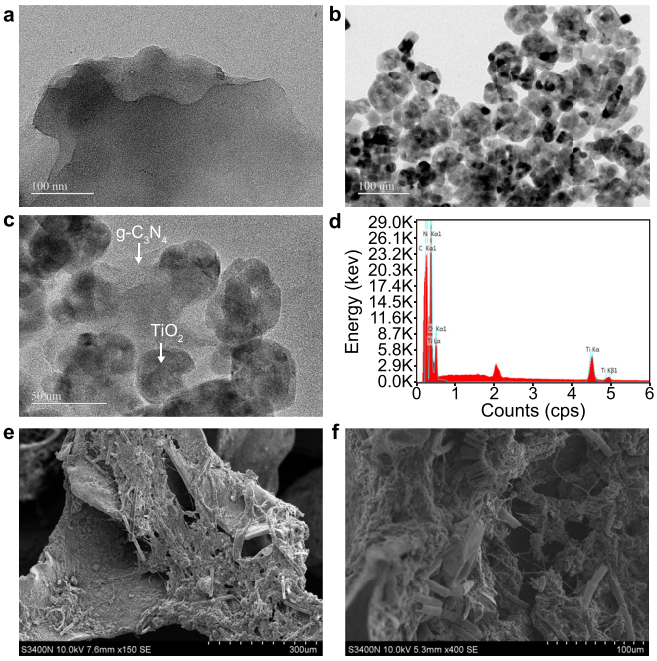

Fig. 2. **a**–**c**, TEM images of bulk g-C_3N_4 (**a**), TiO_2 nanosheet (**b**), and TiO_2/g-C_3N_4 (**c**). **d**, EDS spectrum of TiO_2/g-C_3N_4. **e**–**f**, SEM images of exterior (**e**) and interior (**f**) surface of the sponge carriers.

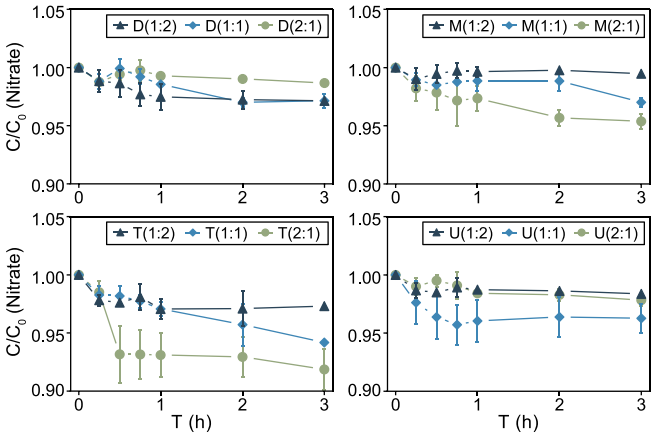

Fig. 3. Nitrate reduction curves of twelve photocatalysts. D: Dicyandiamide; M: Melamine; T: Thiourea; U: Urea; Proportion: TiO_2:g-C_3N_4.

had evaporated. Finally, the carrier loaded with the photocatalyst was sonicated for 5 min and rinsed three times with ultrapure water to remove any unattached photocatalysts that remained on the carrier surface. The sponge carrier loaded with photocatalyst contains 0.46 g TiO_2/g-C_3N_4 g^{-1}.

2.3. Biofilm cultivation

Activated sludge was obtained from the anoxic tank of a sewage treatment plant (114° E, 22° N) in Shenzhen. After settling the sludge for 2 h, remove the supernatant. Inoculation of activated sludge onto catalyst-loaded sponge carriers took place by immersion adsorption for 24 h. Biofilm cultivation was accomplished by placing the carriers in a 500 mL beaker fully wrapped with tin foil. The peristaltic pump was used as a control device to ensure a continuous water flow at 2 mL min^{-1}. Artificial wastewater was equipped according to Table S1. The biofilm was mature and ready for further experiments when the consumption rate of chemical oxygen demand (COD) of the solution in the beaker reached over 70% after about two weeks of sludge cultivation on sponge carriers.

2.4. Reactor setup and experimental protocols

The ICPB reactor consists of a photocatalytic reactor and a xenon lamp (CEL-HXF300, CEAULIGHT). A 300 W Xe lamp was equipped with a filter, which simulates sunlight with a wavelength range of 280–800 nm. The Xe lamp was placed about 10 cm from the top of the reactor, and the reactor received a light intensity of 150 mW cm^{-2}.

As part of an investigation into nitrate reduction processes in ICPB, sponge carriers (without inoculated sludge) loaded with different photocatalysts were used to determine the effects of different photocatalysts on nitrate reduction. Moreover, light and dark comparison experiments, corresponding to ICPB and biodenitrification, were conducted to investigate the effect of different carbon source concentrations on nitrate reduction. The sponge carriers loaded with best-performing photocatalysts and inoculated sludge were used in the comparison experiments. Anoxic conditions were ensured by sampling the water with a syringe at the sampling port. All water samples were filtered through a 0.45 μm membrane. The total volume of the reaction solution was 200 mL. Each experiment was repeated three times.

2.5. Characterization of photocatalysts and bio-carriers

The morphology and surface elemental distribution of photocatalysts were characterized by a scanning electron microscope (SEM, SU8010, Hitachi, Japan) and transmission electron microscopy (TEM, JEM-2100, Japan). The crystal structure of the prepared samples was analyzed by X-ray diffraction (XRD) using an X-ray diffractometer (Empyrean, PANalytical B.V, Netherlands) with a Cu-Kα irradiation source at a scanning speed of 5° min^{-1}. The powder photocatalysts were characterized using Fourier Transform Infrared Spectrometer (FT-IR) spectroscopic characterizations, which were performed utilizing potassium bromide (KBr) disks that supported the powder photocatalysts (Spectrum One, PerkinElmer, USA). UV–vis diffuse reflectance spectra (DRS) of photocatalysts were recorded on a UV-2600 spectrophotometer (Shimadzu Co., Japan). Photoluminescence (PL) spectra were recorded on a FLS 1000 fluorescence spectrophotometer (Edinburgh Instruments, UK).

2.6. Chemical analysis

The ICPB performance was monitored by measuring NO_3^-, NO_2^-, and ammonia (NH_4^+) concentrations using UV spectrophotometry, *N*-(1-naphthyl)-ethylenediamine photometry, and Nessler spectrophotometers, respectively. The total organic carbon (TOC) was measured by a TOC analyzer (Shimadzu TOC-L CPH).

2.7. Metagenomic analysis

To explore the structure and metabolic pathways of the bacteria in the ICPB system, DNA samples of the sludge before running the ICPB system, after the first cycle and third cycle were extracted using FastDNA® SPIN Kit for Soil (MP Biomedicals, Irvine, CA, USA). The high-quality DNA samples were sent to Novogene company (Beijing, China) for metagenomic sequencing. The quality control process resulted in clean reads for downstream analysis. Assembling was carried out using SPAdes (v3.15.3) with the "-meta" option. Species classification was performed with the software

Kracken-bracken using contigs longer than 1000 bp. Prodigal was used to predict open reading frames (ORFs). The ORFs were then included in a non-redundant (NR) gene catalog, which CD-HIT generated with the parameters "-c 0.95, -aS 0.9, -n 9, -G 0, -d 0". A gene abundance (RPKM) calculation was performed by Salmon. Then, the microbial functions and metabolic pathways were analyzed by PICRUSt2 and HUMAnN3. The functional genes were aligned against the Kyoto Encyclopedia of Genes and Genomes (KEGG) database using DIAMOND [2]. In addition, the nitrogen cycling genes were annotated specifically using the NCycDB [29].

The statistical analysis was conducted using the R software (v.4.1.3), and the α-diversity indexes were calculated by the "vegan" R package [22]. The normality of data was evaluated before analysis, and all results were tested for significance. R package ggplot2 [9] was employed for data visualization.

3. Results and discussion

3.1. Characterization of photocatalysts and bio-carriers

The morphology and structure of g-C_3N_4, TiO_2, and TiO_2/g-C_3N_4 nanocomposite were analyzed by SEM and TEM (Fig. 2). TEM imaging reveals that g-C_3N_4 is dense layers to develop a flat massive structure while the TiO_2 is in nanoparticles. After calcination and nanocomposite formation, TiO_2 particles are uniformly distributed on the g-C_3N_4 nanosheets. Energy Dispersive Spectrometer (EDS) results obtained from the TiO_2/g-C_3N_4 composite structure indicate the presence of C, N, O, and Ti elements, suggesting the combination of TiO_2 and g-C_3N_4 has been successfully consolidated. SEM images further demonstrate extensive biofilm growth on both the exterior and interior surfaces of sponge carriers. It is expected that when the sponge is irradiated by simulated solar light, the photocatalyst produces reactive oxygen species that can attack the biofilm on the exterior surface of the sponge. This process results in the shedding of numerous external biofilms, thereby exposing the photocatalyst [47]. However, there is no attack on the internal biofilm due to the protective effect of the sponge, making the ICPB system an ideal one.

The XRD patterns of all four g-C_3N_4 samples (TCN, DCN, MCN, and UCN) show two typical peaks at around 27.4° and 13.1° (Fig. S3). However, the peak intensities of the four g-C_3N_4 samples are different, possibly related to their specific surface areas and nanostructures [40]. The relative intensity of the (002) peak of the g-C_3N_4 component gradually decreased with the increasing loading of TiO_2, which may be due to the dispersion effect of TiO_2 on the g-C_3N_4 nanosheet structure [33]. FT-IR spectra of all four prepared g-C_3N_4 samples show a characteristic vibration model of typical g-C_3N_4 (Fig. S4). With the increasing TiO_2 loading, the peak intensity of TiO_2/g-C_3N_4 composite photocatalyst at 807 cm^{-1} gradually decreased, implying the incorporation of TiO_2 in the triazine framework of g-C_3N_4.

The UV–vis diffuse reflectance spectra (DRS) of MCN, DCN, and UCN have similar absorption edges of about 455 nm (Fig. S5), while TCN has an absorption edge of up to 480 nm. The forbidden bandwidths of the four types of g-C_3N_4 can be obtained by the equation in Supplementary Data. Compared with the band gap of pure TiO_2, the band gaps of all TiO_2/g-C_3N_4 composites are significantly narrower. Among the twelve composites, the one using thiourea as a precursor and prepared with a 2:1 ratio of TiO_2 to g-C_3N_4 (T (2:1)) has the narrowest band gap of 2.38 eV, lower than that of pure g-C_3N_4 (Fig. S6). This can contribute to more separation of photo-generated charge carriers [26]. The four pure g-C_3N_4 have a strong peak at about 460 nm in the PL spectrum (Fig. S7), which can be attributed to the generation of abundant photoinduced charge pairs, resulting in rapid recombination. The PL peak intensities of most TiO_2/g-C_3N_4 have reduced, where T (2:1) has the lowest emission intensity, followed by T (1:1) and M (2:1) (Fig. S7). It indicates that the construction of TiO_2/g-C_3N_4 heterojunction enhances the separation and transfer rate of photogenerated electrons and holes, effectively preventing the carrier complex and enhancing the photocatalytic performance [11,33].

3.2. Performance of nitrate reduction

The nitrate reduction efficiency of different photocatalysts, obtained by compounding g-C_3N_4 prepared from thiourea, melamine, dicyandiamide, and urea as precursors with varying loadings of TiO_2 is shown in Fig. 3. It can be seen that T (2:1), with 8.2% removal rate, is most effective for nitrate reduction. This is followed by T (1:1) and M (2:1), with a removal rate of about 5%. T (1:2), M (1:1), D (1:2), D (1:1), and U (1:1) (D: Dicyandiamide; M: Melamine; T: Thiourea; U: Urea; Proportion: TiO_2:g-C_3N_4) have similar nitrate removal rates of about 3%. The remaining photocatalysts had almost no reduction effect on nitrate. Normally, for a reaction to proceed, electrons must migrate into the conduction band as reducing substances, and their acceptors must have a higher reduction potential than the conduction band [30]. Under visible light irradiation, photo-induced electron transfer from the conduction band of g-C_3N_4 to the conduction band of TiO_2 through the heterojunction of TiO_2 and g-C_3N_4, where the standard potential of the conduction band of TiO_2 is −0.39 eV. The standard potential for reducing NO_3^- to $\cdot NO_3^{2-}$ is E^0 ($NO_3^-/\cdot NO_3^{2-}$) = −0.89 V. Therefore, direct nitrate reduction using the conduction band electrons of TiO_2/g-C_3N_4 is thermodynamically infeasible [41].

Among the twelve photocatalysts, T (2:1), with the highest nitrate reduction efficiency, was chosen as the photocatalyst in ICPB.

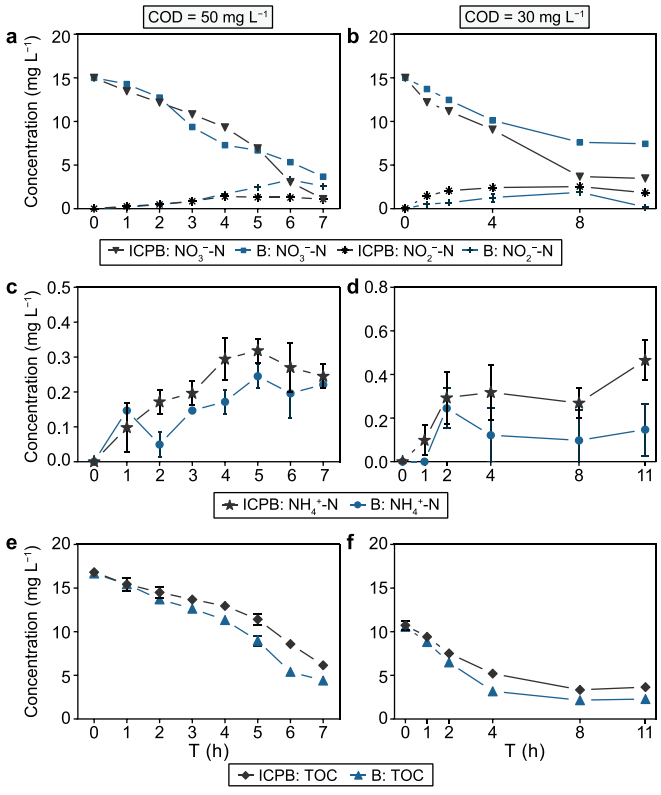

Fig. 4. Concentration variation of NO_3^-, NO_2^- (**a**, **b**), NH_4^+ (**c**, **d**), and TOC (**e**, **f**) in ICPB with an initial COD of 50 mg L^{-1} (**a**, **c**, **e**) and 30 mg L^{-1} (**b**, **d**, **f**). ICPB: biodegradation and photocatalysis; B: biodegradation.

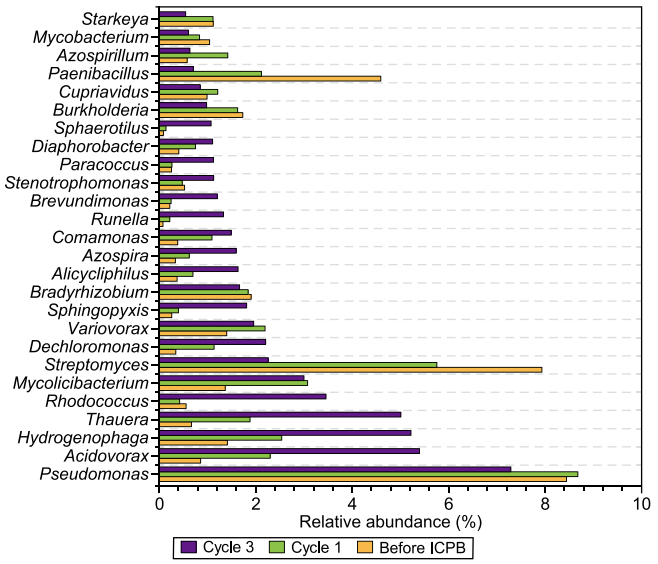

Fig. 5. Predominant bacteria genera with relative abundances (RPKM) of more than 1%.

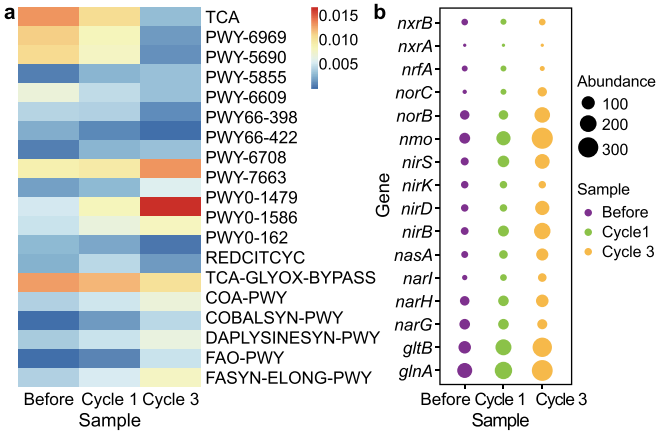

Fig. 6. The variation of metabolic pathways (**a**) and functional genes (**b**) about nitrogen metabolism.

Fig. 4a and b compares the nitrate reduction effect under ICPB and biodegradation conditions, with COD content of 50 and 30 mg L^{-1}, respectively. The initial concentration of nitrate in the solution is 15 mg L^{-1}. When the carbon source concentration is high, the nitrate reduction rate after 7 h of ICPB reaction is 92.6%. As denitrifying bacteria are mostly heterotrophic microorganisms, they can maintain their own growth and complete the denitrification process under sufficient carbon sources. Therefore, even with biodegradation alone, a nitrate reduction rate of 75.6% can be achieved. However, the rate of bio-denitrification slowed down after 5 h of reaction. The phenomenon is attributed to the large consumption of available carbon sources in the wastewater and the decrease in the number of electron acceptors available for denitrifying bacteria, leading to the inhibition of denitrification. The ICPB, however, did not experience any changes in nitrate reduction rate. This may be due to some denitrifying bacteria that utilize photoelectrons to maintain the denitrification process [49]. The advantage of ICPB was more obvious when the COD concentration was reduced to 30 mg L^{-1} (Fig. 4b). The findings indicate that after an 8-h reaction period, the nitrate reduction efficiency of ICPB was 75.6%, while it was only 49.3% by bio-denitrification. Clearly, ICPB is more effective and stable for nitrate removal, which has a higher nitrate removal rate even when the concentration of carbon source is insufficient.

To further investigate the effect of carbon source concentration on the nitrate reduction performance, the concentrations of nitrite nitrogen and ammonium nitrogen were determined during the nitrate reduction process. Nitrite is the first stable intermediate product generated by nitrate reduction and is present in the solution or further reduced to N_2 or NH_4^+. When the COD was 50 mg L^{-1}, it was found that after 6 h of bio-denitrification, the concentration of nitrite nitrogen in the solution peaked at 3.32 mg L^{-1} and did not decrease significantly at the end of the experiment. However, in ICPB, the concentration of nitrite nitrogen slightly increased to 1.41 mg L^{-1} at 4 h and then decreased to 1.11 mg L^{-1} in the next 3 h (Fig. 4a). It is apparent that ICPB has a certain inhibitory effect on nitrite accumulation. It has been reported that the accumulation of nitrite nitrogen may increase nitrous oxide emissions. This is because a higher concentration of nitrite nitrogen can produce more molecular ammonia and free nitrite (FNA), while the latter can inhibit the nitrous oxide reductase activity [49]. Therefore, ICPB reduced the release of nitrous oxide during nitrate reduction. However, when the COD was reduced to 30 mg L^{-1}, the amount of nitrite produced by ICPB was more than that by bio-denitrification (Fig. 4b). As nitrate was reduced, the concentration of nitrite nitrogen gradually increased, reaching a maximum at 8 h, and then gradually decreased over the next 3 h. Possibly, it is because nitrite-reducing bacteria are heterotrophic microorganisms and, therefore, unable to utilize photoelectrons effectively. The nitrite reduction process can only be accomplished using the carbon source in the wastewater as an electron acceptor. Therefore, a low concentration of organic carbon is not conducive to reducing nitrite. Additionally, the ICPB system exhibits a greater nitrate reduction than bio-denitrification, resulting in a higher nitrite accumulation. Thus, appropriately increasing the carbon source concentration in ICPB could suppress nitrite accumulation.

Nitrate reduction is a step-wise process in which ammonium is a by-product after nitrite generation [8]. Small amounts of ammonium were produced during the reactions (Fig. 4c,d). The slightly higher concentration of ammonium in ICPB may be due to the involvement of the photocatalytic reaction in the reduction process after nitrite generation.

In addition to nitrite and ammonium nitrogen, nitrogen gas is also a major product of nitrate reduction. The photocatalytic selectivity of nitrogen can be calculated from the equation below:

$$S(N_2) = \frac{[NO_3^-]_0 - [NO_3^-]_t - [NO_2^-]_t - [NH_4^+]_t}{[NO_3^-]_0 - [NO_3^-]_t} \times 100\%$$

where $S(N_2)$ denotes the selectivity of N_2, $[NO_3^-]_0$ and $[NO_3^-]_t$ denote the nitrate concentration at moments 0 and t, and $[NO_2^-]_t$ and $[NH_4^+]_t$ denote the nitrite and ammonium concentrations at moment t. According to the equation, when the COD was 50 mg L^{-1}, after 7 h of reaction, the conversion of N_2 was 93.6% and 82.6% in ICPB and bio-denitrification, respectively. The ICPB system improved the N_2 conversion by 11%, effectively reducing the number of undesirable products. However, when COD was 30 mg L^{-1}, the N_2 conversion of ICPB decreased to 86.44%, which may be due to the greater accumulation of intermediate products of nitrite (Fig. 4b). Therefore, the higher initial organic carbon concentration could facilitate the conversion of nitrate to nitrogen during denitrification process.

The TOC was measured during the experiment to investigate using photoelectrons by ICPB. When the concentration of carbon source was higher (COD = 50 mg L^{-1}, Fig. 4e), the TOC consumption

of ICPB and bio-denitrification were 63.3% and 73.6%, respectively, and less organic carbon source was utilized by ICPB. At the first hour of the reaction, the TOC consumption of both systems was essentially the same, while the nitrate reduction rate of ICPB was higher than that of bio-denitrification (Fig. 4a). After 5 h of reaction, ICPB had a more pronounced nitrate reduction effect, and the TOC consumption was still lower than that of bio-denitrification. When the carbon source concentration was lower (COD = 30 mg L^{-1}, Fig. 4f), ICPB consistently maintained lower organic carbon consumption and higher nitrate reduction efficiency (Fig. 4b–f). The ICPB with a higher starting carbon source concentration had better nitrate reduction rates when the TOC concentration was reduced from 10 to 8 mg L^{-1}. This may be due to the thicker biofilm at higher concentrations of carbon sources, which can act as a hole scavenger for photocatalytic denitrification, collecting electrons generated by the photocatalyst for metabolism and promoting nitrate reduction [49]. It can be seen that ICPB has a cutting edge in using less organic carbon to reduce more nitrate than biodegradation, regardless of the change in carbon source concentration. This increase in nitrate reduction efficiency proved to be a step forward for the process and opened up new possibilities for further optimization.

3.3. Structure changes in microbial community

The α-diversity of the bacterial community was assessed using the indexes of Chao-1, ACE, and Pielou (Table S2). Chao 1, Pielou, and ACE indices decreased after ICPB, which indicated that the richness and evenness of the microbial community decreased and the functional bacterial might be enriched. Bacterial diversity was overviewed at the phylum (Fig. S2) and genus level (Fig. 5). There was no significant difference in the bacterial community structure at the phylum level before and after ICPB. The dominant phyla were Proteobacteria, Actinobacteria, Firmicutes, Bacteroidetes, and Planctomycetes. These five phyla occupied 94.8%, 95.8%, and 97.7% of the total bacteria abundance before ICPB, cycle 1, and cycle 3, respectively. In particular, the proportion of Proteobacteria gradually increased from 57% to 75.1%. It indicated that the community was dominated by Proteobacteria, closely related to denitrification in sewage treatment systems according to previous research [50].

At the genus level, *Pseudomonas* dominated the ICPB system before and after the reaction. *Pseudomonas* exhibit remarkable diversity in carbon source utilization and nitrogen cycling, especially excelling in the degradation of nitrates [10,31,39,44]. The abundances of *Acidovorax*, *Thauera*, *Hydrogenophaga*, and *Rhodococcus* significantly increased after ICPB. *Acidovorax* and *Thauera* were identified as denitrifying bacteria carrying *NarG* and *NirS* [27]. *Hydrogenophaga* was a type of facultative autotroph, and some species (*Hydrogenophaga pseudofalva* and *Hydrogenophaga taeniospiralis*) could denitrification and anaerobic nitrate respiration [18]. *Dechloromonas*, *Sphingopyxis*, *Alicycliphilus*, *Azospira*, *Comamonas*, *Runella*, *Brevundimonas*, *Stenotrophomonas*, *Paracoccus*, *Diaphorobacter*, and *Sphaerotilus* became the top 1% of the genus. However, the abundance of *Streptomyces* decreased most significantly from 7.9% to 2.3% after ICPB. Overall, the bacterial community was more favorable for denitrification and nitrate reduction after ICPB.

3.4. The metabolic mechanism of nitrate in ICPB

The abundance of nitrogen metabolism pathway (ko00910) significantly increased by 422% and 600% after ICPB cycle 1 and cycle 3, respectively (Fig. S1). There were some changes of other metabolic pathways after ICPB (Fig. 6a). The abundance of pathways PWY-7663 and PWY0-1586, which were associated with gondoate biosynthesis (anaerobic) and peptidoglycan maturation (*meso*-diaminopimelate containing), was increased after ICPB

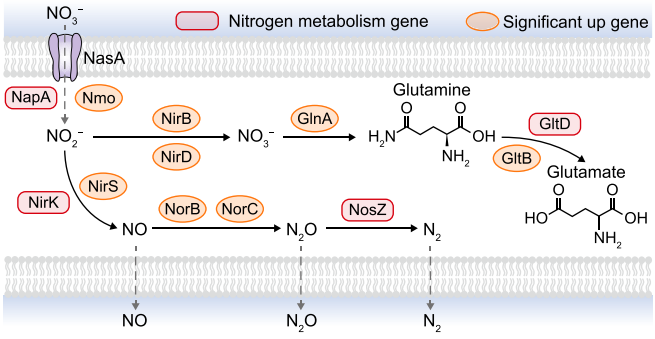

Fig. 7. Proposed metabolic model of nitrate reduction in ICPB.

reactions. The abundance of pathways associated with the tricarboxylic acid cycle (TCA) was reduced. Pathways PWY-5690 and PWY-6969 were indicated as TCA cycle II and TCA cycle V (2-oxoglutarate synthase), respectively. A prior report has shown that the TCA cycle could provide reducing power for nitrate reduction [45]. The reduced energy supply from the TCA cycle also provides favorable evidence for the ICPB's capability to efficiently remove nitrate under low-carbon conditions.

To further explore the nitrogen metabolism functional changes in the microbial community, we quantified nitrogen cycle-related genes using the NCycDB database. A significant increase in the abundance of some functional genes related to the nitrogen cycle was observed after ICPB performance (Fig. 6b). The abundances of *glnA*, *nmo*, and *gltB* (gs__K00265) increased by 119%, 402%, and 210%. Due to diverse functional genes in different bacteria, changes in microbial community structure can significantly impact the variation of functional genes. *GlnA* was glutamine synthetase and related to nitrogen regulatory P-II. *Nmo* was nitronate monooxygenase and related to biodegradation. *GltB* was a glutamate synthase (NADPH/NADH) large chain [29]. Notably, the abundance of *norB*, *nirS*, *nirD*, and *nirB* also increased after ICPB. *NorB* and *nirS* were typical denitrifying enzymes. *NorB* was nitric oxide reductase subunit B, and *nirS* was nitrite reductase (NO-forming) [45]. *NirD* and *nirB* were nitrite reductase (NADH) small and large subunits, respectively [29]. Therefore, a possible nitrate metabolic pathway in the ICPB system was proposed (Fig. 7). Through quantitative analysis of the denitrification metabolism-related genes, the potential of the ICPB system for nitrogen removal could be proved at the gene level, which was conducive to further study of the mechanism of ICPB denitrification. This study represents the first application of metagenomics to analyze the microbial community structure and metabolic pathways involved in nitrate degradation within the ICPB system. It's worth mentioning that although metagenomics has advantages in analyzing functional genes, especially for uncultivable complex microbial communities, it has certain limitations in characterizing metabolic functional phenotypes and requires supplementation based on metabolomic data. Future investigations will endeavor to integrate multiple approaches to enhance our comprehension of microbial interactions and electron transfer mechanisms within the ICPB system.

4. Conclusions

Compared with traditional biodegradation, ICPB can improve nitrate reduction efficiency by 17% and nitrogen conversion efficiency by 11%. Moreover, this approach requires 12.2% less organic carbon to achieve a 26.3% greater nitrate reduction under low organic carbon conditions. With increased ICPB cycles, the system's microbial community and metabolic pathway evolved in the

direction of nitrate reduction. The microbial analysis results indicate that microorganisms can capture the photons generated by photocatalysis to maintain their metabolism and reduce nitrate. This study provides the scientific basis and technical support for nitrate reduction in ICPB under hypotrophic conditions.

CRediT authorship contribution statement

Bingjie Xue: Conceptualization, Investigation, Formal Analysis, Writing - Original Draft, Writing - Review & Editing. **Li Tian:** Data Curation, Writing - Original Draft, Writing - Review & Editing. **Yaqi Liu:** Conceptualization, Methodology, Data Curation. **Lingxiu Peng:** Data Curation. **Waheed Iqbal:** Writing - Review & Editing. **Liangzhong Li:** Conceptualization, Writing - Review & Editing. **Yanping Mao:** Conceptualization, Funding Acquisition, Writing - Review & Editing.

Declaration of competing interest

The authors declare that they have no known competing financial interests or personal relationships that could have appeared to influence the work reported in this paper.

Acknowledgement

This work was supported by the Natural Science Foundation of Guangdong Province, China (2022A1515011961, 2023A1515012019); the Stable Support Program of Colleges and Universities in Shenzhen, China (20200813153536001).

Appendix A. Supplementary data

Supplementary data to this article can be found online at https://doi.org/10.1016/j.ese.2024.100390.

References

[1] N. Barrabés, J. Sá, Catalytic nitrate removal from water, past, present and future perspectives, Appl. Catal., B 104 (2011) 1–5.
[2] B. Buchfink, C. Xie, D.H. Huson, Fast and sensitive protein alignment using DIAMOND, Nat. Methods 12 (2015) 59–60.
[3] H. Cai, L. Sun, Y. Wang, T. Song, M. Bao, X. Yang, Unprecedented efficient degradation of phenanthrene in water by intimately coupling novel ternary composite Mn_3O_4/MnO_2-Ag_3PO_4 and functional bacteria under visible light irradiation, Chem. Eng. J. 369 (2019) 1078–1092.
[4] M. Chen, X.-F. Zhou, Y.-Q. Yu, X. Liu, R.J.-X. Zeng, S.-G. Zhou, Z. He, Light-driven nitrous oxide production via autotrophic denitrification by self-photosensitized Thiobacillus denitrificans, Environ. Int. 127 (2019) 353–360.
[5] M. Dalmau, I. Rodriguez-Roda, E. Ayesa, J. Odriozola, L. Sancho, J. Comas, Development of a decision tree for the integrated operation of nutrient removal MBRs based on simulation studies and expert knowledge, Chem. Eng. J. 217 (2013) 174–184.
[6] R. Ding, W. Yan, Y. Wu, Y. Xiao, H. Gang, S. Wang, L. Chen, F. Zhao, Light-excited photoelectrons coupled with bio-photocatalysis enhanced the degradation efficiency of oxytetracycline, Water Res. 143 (2018) 589–598.
[7] S. Dong, S. Dong, X. Tian, Z. Xu, D. Ma, B. Cui, N. Ren, B.E. Rittmann, Role of self-assembly coated Er^{3+}:$YAlO_3/TiO_2$ in intimate coupling of visible-light-responsive photocatalysis and biodegradation reactions, J. Hazard Mater. 302 (2016) 386–394.
[8] K. Doudrick, T. Yang, K. Hristovski, P. Westerhoff, Photocatalytic nitrate reduction in water: managing the hole scavenger and reaction by-product selectivity, Appl. Catal., B 136 (2013) 40–47.
[9] C. Ginestet, ggplot2: Elegant Graphics for Data Analysis, Oxford University Press, 2011.
[10] X. Huang, C.G. Weisener, J. Ni, B. He, D. Xie, Z. Li, Nitrate assimilation, dissimilatory nitrate reduction to ammonium, and denitrification coexist in Pseudomonas putida Y-9 under aerobic conditions, Bioresour. Technol. 312 (2020) 123597.
[11] K. Jiang, W. Iqbal, B. Yang, M. Rauf, I. Ali, X. Lu, Y. Mao, Noble metal-free $NiCo_2S_4$/CN sheet-on-sheet heterostructure for highly efficient visible-light-driven photocatalytic hydrogen evolution, J. Alloys Compd. 853 (2021) 157284.
[12] B. Li, J.D. Sun, C. Tang, Z.Y. Yan, J. Zhou, X.Y. Wu, H.H. Jia, X.Y. Yong, A novel core-shell Fe@Co nanoparticles uniformly modified graphite felt cathode (Fe@Co/GF) for efficient bio-electro-Fenton degradation of phenolic compounds, Sci. Total Environ. 760 (2021) 143415.
[13] G. Li, S. Park, D.-W. Kang, R. Krajmalnik-Brown, B.E. Rittmann, 2,4,5-Trichlorophenol degradation using a novel TiO_2-coated biofilm carrier: roles of adsorption, photocatalysis, and biodegradation, Environ. Sci. Technol. 45 (2011) 8359–8367.
[14] G. Li, S. Park, B.E. Rittmann, Degradation of reactive dyes in a photocatalytic circulating-bed biofilm reactor, Biotechnol. Bioeng. 109 (2012) 884–893.
[15] G. Li, S. Park, B.E. Rittmann, Developing an efficient TiO_2-coated biofilm carrier for intimate coupling of photocatalysis and biodegradation, Water Res. 46 (2012) 6489–6496.
[16] K. Liu, J. Chen, F. Sun, J. Yu, X. Zhang, Y. Xu, Y. Liu, M. Tang, Y. Yang, Enhanced degradation of azo dyes wastewater by S-scheme heterojunctions photocatalyst g-C3N4/MoS2 intimately coupled Rhodopseudomonas palustris with chitosan modified polyurethane sponge carrier, Int. J. Hydrogen Energy 48 (2023) 22319–22333.
[17] K. Liu, Y. Yang, F. Sun, Y. Liu, M. Tang, J. Chen, Rapid degradation of Congo red wastewater by Rhodopseudomonas palustris intimately coupled carbon nanotube - silver modified titanium dioxide photocatalytic composite with sodium alginate, Chemosphere 299 (2022) 134417.
[18] X. Liu, M. Huang, S. Bao, W. Tang, T. Fang, Nitrate removal from low carbon-to-nitrogen ratio wastewater by combining iron-based chemical reduction and autotrophic denitrification, Bioresour. Technol. 301 (2020) 122731.
[19] D.D. Luiz, S.L.F. Andersen, C. Berger, H.J. Jose, R. Moreira, Photocatalytic reduction of nitrate ions in water over metal-modified TiO_2, J. Photochem. Photobiol. Chem. 246 (2012) 36–44.
[20] Y. Ma, H. Xiong, Z. Zhao, Y. Yu, D. Zhou, S. Dong, Model-based evaluation of tetracycline hydrochloride removal and mineralization in an intimately coupled photocatalysis and biodegradation reactor, Chem. Eng. J. 351 (2018) 967–975.
[21] V.N. Montesinos, N. Quici, H. Destaillats, M.I. Litter, Nitric oxide emission during the reductive heterogeneous photocatalysis of aqueous nitrate with TiO_2, RSC Adv. 5 (2015) 85319–85322.
[22] J. Oksanen, R. Kindt, P. Legendre, B. O'Hara, M.H.H. Stevens, M.J. Oksanen, M. Suggests, The vegan package, Community Ecology Package 10 (2007) 719.
[23] Z. Qin, Z. Zhao, W. Jiao, Z. Han, L. Xia, Y. Fang, S. Wang, L. Ji, Y. Jiang, Coupled photocatalytic-bacterial degradation of pyrene: removal enhancement and bacterial community responses, Environ. Res. 183 (2020) 109135.
[24] K.K. Sakimoto, A.B. Wong, P. Yang, Self-photosensitization of non-photosynthetic bacteria for solar-to-chemical production, Science 351 (2016) 74–77.
[25] K. Sathishkumar, S. Naraginti, K. Lavanya, F. Zhang, R. Ayyamperumal, X. Liu, Intimate coupling of gC3N4/CdS semiconductor on eco-friendly biocarrier loofah sponge for enhanced detoxification of ciprofloxacin, Environ. Res. 235 (2023) 116558.
[26] R.A. Senthil, J. Theerthagiri, A. Selvi, J. Madhavan, Synthesis and characterization of low-cost g-C_3N_4/TiO_2 composite with enhanced photocatalytic performance under visible-light irradiation, Opt. Mater. 64 (2017) 533–539.
[27] E. Stackebrandt, F.A. Rainey, N.L. WardRainey, Proposal for a new hierarchic classification system, Actinobacteria classis nov, Int. J. Syst. Bacteriol. 47 (1997) 479–491.
[28] M. Sui, Y. Li, Y. Jiang, Y. Zhang, L. Wang, W. Zhang, X. Wang, Light exposure interferes with electroactive biofilm enrichment and reduces extracellular electron transfer efficiency, Water Res. 188 (2021) 116512.
[29] Q. Tu, L. Lin, L. Cheng, Y. Deng, Z. He, NCycDB: a curated integrative database for fast and accurate metagenomic profiling of nitrogen cycling genes, Bioinformatics 35 (2019) 1040–1048.
[30] H.O.N. Tugaoen, S. Garcia-Segura, K. Hristovski, P. Westerhoff, Challenges in photocatalytic reduction of nitrate as a water treatment technology, Sci. Total Environ. 599–600 (2017) 1524–1551.
[31] L. Wang, C. Chen, Y. Tang, B. Liu, A novel hypothermic strain, Pseudomonas reactans WL20-3 with high nitrate removal from actual sewage, and its synergistic resistance mechanism for efficient nitrate removal at 4 °C, Bioresour. Technol. 385 (2023) 129389.
[32] Y. Wang, C. Chen, D. Zhou, H. Xiong, Y. Zhou, S. Dong, B.E. Rittmann, Eliminating partial-transformation products and mitigating residual toxicity of amoxicillin through intimately coupled photocatalysis and biodegradation, Chemosphere 237 (2019) 124491.
[33] K. Wei, K. Li, L. Yan, S. Luo, H. Guo, Y. Dai, X. Luo, One-step fabrication of g-C_3N_4 nanosheets/TiO_2 hollow microspheres heterojunctions with atomic level hybridization and their application in the multi-component synergistic photocatalytic systems, Appl. Catal., B 222 (2018) 88–98.
[34] H. Xiong, S. Dong, J. Zhang, D. Zhou, B.E. Rittmann, Roles of an easily biodegradable co-substrate in enhancing tetracycline treatment in an intimately coupled photocatalytic-biological reactor, Water Res. 136 (2018) 75–83.
[35] J. Xiong, S. Guo, T. Zhao, Y. Liang, J. Liang, S. Wang, H. Zhu, L. Zhang, J.R. Zhao, G. Chen, Degradation of methylene blue by intimate coupling photocatalysis and biodegradation with bagasse cellulose composite carrier, Cellulose 27 (2020) 3391–3404.
[36] N. Yan, L. Chang, L. Gan, Y. Zhang, R. Liu, B.E. Rittmann, UV photolysis for accelerated quinoline biodegradation and mineralization, Appl. Microbiol. Biotechnol. 97 (2013) 10555–10561.
[37] L. Yang, Y. Zhang, Q. Bai, N. Yan, H. Xu, B.E. Rittmann, Intimately coupling of photolysis accelerates nitrobenzene biodegradation, but sequential coupling

slows biodegradation, J. Hazard Mater. 287 (2015) 252–258.
[38] X. Yang, X. Qi, G. Ma, Z. Li, Q. Liu, S. Khan, Y. Zhao, L. Zhang, Z. Geng, Y. Guo, Novel Z-Scheme Ag/TiO_2/AgMIL-101(Cr) as an efficient photocatalyst for nitrogen production from nitrate, Appl. Surf. Sci. 479 (2019) 1048–1056.
[39] D. Zhang, Y. Liu, Y. Han, Y. Zhang, X. Jia, W. Li, D. Li, L. Jing, Nitrate removal from low C/N wastewater at low temperature by immobilized Pseudomonas sp. Y39-6 with versatile nitrate metabolism pathways, Bioresour. Technol. 326 (2021) 124794.
[40] G.G. Zhang, J.S. Zhang, M.W. Zhang, X.C. Wang, Polycondensation of thiourea into carbon nitride semiconductors as visible light photocatalysts, J. Mater. Chem. 22 (2012) 8083–8091.
[41] H. Zhang, Z. Liu, Y. Li, C. Zhang, Y. Wang, W. Zhang, L. Wang, L. Niu, P. Wang, C. Wang, Intimately coupled TiO_2/g-C_3N_4 photocatalysts and in-situ cultivated biofilms enhanced nitrate reduction in water, Appl. Surf. Sci. 503 (2020) 144092.
[42] H. Zhang, Y. Lu, Y. Li, C. Wang, Y. Yu, W. Zhang, L. Wang, L. Niu, C. Zhang, Propelling the practical application of the intimate coupling of photocatalysis and biodegradation system: system amelioration, environmental influences and analytical strategies, Chemosphere 287 (2022) 132196.
[43] L. Zhang, Z. Xing, H. Zhang, Z. Li, X. Wu, X. Zhang, Y. Zhang, W. Zhou, High thermostable ordered mesoporous SiO_2–TiO_2 coated circulating-bed biofilm reactor for unpredictable photocatalytic and biocatalytic performance, Appl. Catal., B 180 (2016) 521–529.
[44] W. Zhang, J. Shen, H. Zhang, C. Zheng, R. Wei, Y. Gao, L. Yang, Efficient nitrate removal by Pseudomonas mendocina GL6 immobilized on biochar, Bioresour. Technol. 320 (2021) 124324.
[45] Z. Zhang, Y. Zhang, Y. Chen, Comparative metagenomic and metatranscriptomic analyses reveal the functional species and metabolic characteristics of an enriched denitratation community, Environ. Sci. Technol. 54 (2020) 14312–14321.
[46] H. Zhao, S. Chen, X. Quan, H. Yu, H. Zhao, Integration of microfiltration and visible-light-driven photocatalysis on g-C_3N_4 nanosheet/reduced graphene oxide membrane for enhanced water treatment, Appl. Catal., B 194 (2016) 134–140.
[47] D. Zhou, Z. Xu, S. Dong, M. Huo, S. Dong, X. Tian, B. Cui, H. Xiong, T. Li, D. Ma, Intimate coupling of photocatalysis and biodegradation for degrading phenol using different light types: visible light vs UV light, Environ. Sci. Technol. 49 (2015) 7776–7783.
[48] D. Zhou, Z. Xu, S. Dong, M. Huo, S. Dong, X. Tian, B. Cui, H. Xiong, T. Li, D. Ma, Intimate coupling of photocatalysis and biodegradation for degrading phenol using different light types: visible light vs UV light, Environ. Sci. Technol. 49 (2015) 7776–7783.
[49] N. Zhu, J. Tang, C. Tang, P. Duan, L. Yao, Y. Wu, D.D. Dionysiou, Combined CdS nanoparticles-assisted photocatalysis and periphytic biological processes for nitrate removal, Chem. Eng. J. 353 (2018) 237–245.
[50] N.Y. Zhu, Y.H. Wu, J. Tang, P.F. Duan, L.G. Yao, E.R. Rene, P.K. Wong, T.C. An, D.D. Dionysiou, A new concept of promoting nitrate reduction in surface waters: simultaneous supplement of denitrifiers, electron donor pool, and electron mediators, Environ. Sci. Technol. 52 (2018) 8617–8626.